J Appl Physiol 95: 1926–1936, 2003.
First published July 18, 2003; 10.1152/japplphysiol.00102.2003.

Lung and alveolar wall elastic and hysteretic behavior in rats: effects of in vivo elastase treatment

Kelly K. Brewer,[1] Hiroaki Sakai,[1] Adriano M. Alencar,[1] Arnab Majumdar,[1,2] Stephen P. Arold,[1] Kenneth R. Lutchen,[1] Edward P. Ingenito,[3] and Béla Suki[1]
[1]*Department of Biomedical Engineering and* [2]*Center for Polymer Studies, Department of Physics, Boston University; and* [3]*Brigham and Women's Hospital, Boston, Massachusetts 02215*

Submitted 31 January 2003; accepted in final form 11 July 2003

Brewer, Kelly K., Hiroaki Sakai, Adriano M. Alencar, Arnab Majumdar, Stephen P. Arold, Kenneth R. Lutchen, Edward P. Ingenito, and Béla Suki. Lung and alveolar wall elastic and hysteretic behavior in rats: effects of in vivo elastase treatment. *J Appl Physiol* 95: 1926–1936, 2003. First published July 18, 2003; 10.1152/japplphysiol.00102.2003.—We investigated the relationship between the microscopic elastic and hysteretic behavior of the alveolar walls and the macroscopic mechanical properties of the whole lung in an in vivo elastase-treated rat model of emphysema. We measured the input impedance of isolated lungs at three levels of transpulmonary pressure (Ptp) and used a linear model to estimate the dynamic elastance and hysteresivity of the lungs. The elastance of the normal lungs increased steeply with Ptp, whereas this dependence diminished in the treated lungs. Hysteresivity decreased significantly with Ptp in the normal lungs, but this dependence disappeared in the treated lungs. To investigate the microscopic origins of these changes, the alveolar walls were immunofluorescently labeled in small tissue strips. By using a fluorescent microscope, the lengths and angular orientations of individual alveolar walls were followed during cyclic uniaxial stretching of the tissue strips. The microstrains (relative change in segment length) and changes in angle of the alveolar walls showed considerable heterogeneity, which was interpreted in terms of a network model. In the normal strips, the alveolar walls showed larger angular changes compared with the treated tissue, whereas the alveolar walls of the treated tissue tended to be more extensible. Hysteresis in the average angle change was also larger in the treated tissue than in the normal tissue. We conclude that the decreased Ptp dependence of elastance and the constant hysteresivity in the treated lungs are related to microstructural remodeling and network phenomena at the level of the alveolar walls.

collagen; elastin; fluorescent imaging; remodeling; mechanics

EMPHYSEMA IS THOUGHT TO RESULT from the combined effects of inflammation and an imbalance of protease and antiprotease activity in the lung (1, 9, 29). Collagen and elastin, the main load-bearing fibers in the parenchyma, undergo remodeling during emphysema, and the remodeled fiber network has altered mechanical properties (7, 17, 33). Additionally, the mechanical forces applied to the lung during normal breathing can contribute to progressive destruction of remodeled alveolar walls (11), resulting in further loss of elastic recoil of the lung and a decreased surface area for gas exchange (4, 10). The functional consequences of tissue destruction and remodeling in emphysema can be evaluated by organ-level measurements such as lung resistance and elastance.

Many studies have investigated the microscopic determinants of lung elastance in the normal lung (5, 18, 21, 31, 35, 36). Surface film is an important contributor to elastance, both directly and indirectly via parenchymal distortion (22). The effects of mechanical interdependence on lung elasticity were examined by using a hexagonal spring network (15), and subsequently continuum analysis was used to describe the effects of this interdependence on the small strain behavior of the network (34). Experimentally, topological studies of lung tissue have characterized the mechanical connections between connective tissue cables and septal membranes in the elastic network of the alveolar parenchyma (24). In conjunction with these studies, analysis of the structure over a range of lung volumes allows inferences to be made about how configuration affects the elastic properties of the tissue. For example, angles measured at the distinctive junctions where two septa meet have been found to be consistent with the principle of surface area minimization (3). Additionally, microstrains averaged over several alveoli appeared to follow macrostrain (2). Thus the study of microscopic elastic behavior may provide key information about the origins of macroscopic elastance.

Although the microscopic properties of the parenchymal network influence the elastance of the lung, resistive properties are also important determinants of lung function. Lung tissue resistance appears to be a major component of total lung resistance in many species around the breathing frequencies (6, 8, 13). Hysteresis, which can be measured as the area enclosed by a pressure-volume loop of the lung, is closely related to tissue resistance (6). Potential sources of hysteresis in the normal lung include dynamic properties of surfactant at the air-liquid interface (16, 22), contractile cells (e.g., smooth muscle and/or myofibroblasts) (5), and the behavior of the collagen-elastin network surrounding

Address for reprint requests and other correspondence: B. Suki, Dept. of Biomedical Engineering, Boston Univ., 44 Cummington St., Boston, MA 02215 (E-mail: bsuki@bu.edu).

The costs of publication of this article were defrayed in part by the payment of page charges. The article must therefore be hereby marked "*advertisement*" in accordance with 18 U.S.C. Section 1734 solely to indicate this fact.

the alveoli (19, 36). It has been suggested that surface forces play a role in parenchymal mechanics, and tissue distortion at the alveolar level may be an important contributor of tissue resistance (22). However, dynamic oscillations invoking small changes in surface area of a surfactant monolayer have shown negligible hysteresis in the surfactant itself (27). Indeed, others (35) have also argued that parenchymal mechanics are largely dominated by the connective tissues. To characterize hysteretic properties of the lung, Fredberg and Stamenovic (6) introduced hysteresivity, an intensive property of the tissue defined as the ratio of dissipated energy to stored energy over a cycle. Since hysteresivity is a material property at the macroscopic level, it should depend on the composition and microstructure of the tissue. However, it still remains unclear how microscopic alterations of the connective tissue lead to deterioration in macroscopic lung function during emphysema.

We hypothesized that during emphysema, degradation and remodeling of the connective tissue matrix lead to microscopic alterations of the alveolar walls, which are reflected in lung tissue elastance and hysteresivity. To test this hypothesis, we analyzed the mechanical behavior of lung tissue on both macroscopic and microscopic levels in normal and elastase-treated rats. We then associated changes in organ level elastic and hysteretic behavior with changes in alveolar wall mechanics. Specifically, the contribution of the collagen-elastin network to organ-level elastance and hysteresivity was assessed by immunofluorescently labeling the alveolar walls in normal and emphysematous tissue strips and imaging the alveolar walls during deformations similar in magnitude to those occurring during breathing.

EXPERIMENTAL PROCEDURES

Two groups of male Sprague-Dawley rats (Charles River Laboratories, Boston, MA) weighing between 280 and 350 g were anesthetized by intraperitoneal injection of 10–20 mg/kg xyalzine and 30–35 mg/kg ketamine (protocol approved by Boston University and Harvard Medical School Animal Care and Use Committee). The rats were treated by a single intratracheal instillation of 1 ml of either physiological saline for the normal control group ($n = 5$) or 2 IU of porcine pancreatic elastase (Sigma Chemical, St. Louis, MO) to develop an emphysematous group ($n = 5$) (30). The normal group was a subset of those animals used by Sakai et al. (26). After 4 wk, the animals were anesthetized and the chest was opened. The animals were exsanguinated by cutting the portal vein and abdominal aorta, and the lungs were perfused with saline and heparin (1,000 IU/l) to remove the remaining blood from the pulmonary vasculature. The lungs were then isolated from the thoracic cavity, and a tracheal cannula (2 mm inner diameter) was connected to the outlet of a computer-controlled small-animal ventilator (Flexivent; SCIREQ). Impedance data were collected by superimposing forced oscillations on static transpulmonary pressures (Ptp) of 3, 8, and 11 cmH_2O while the lungs were floating in a saline bath. Macroscopic mechanical parameters were calculated from these data, and tissue strips were isolated from the lungs for microscopic measurements.

Impedance measurements. Impedance data were collected by using the optimal ventilator waveform (OVW) (14). The OVW is a broadband waveform that contains energy at frequencies from 0.5 to 15 Hz and consists of frequencies selected to eliminate harmonic distortion and minimize cross-talk among the input frequencies. The OVW method provides information on the mechanical properties of the lung while delivering physiological tidal volumes of 10 ml/kg in a closed-circuit, forced-oscillatory system (14).

Macroscopic measurements. The volume displacement and pressure signals from the ventilator were low-pass filtered at 30 Hz and sampled at 256 Hz before being stored. With the use of Fourier analysis, impedance spectra were calculated on overlapping blocks of pressure and flow data as the ratio of the cross-power spectrum of pressure and flow and the auto-power spectrum of flow. Lung mechanics data from the isolated lungs were analyzed by using an inhomogeneous linear model introduced by Suki et al. (32). In this model, the airway tree consists of multiple airway compartments arranged in parallel. Each compartment is comprised of a resistance (R), an inertance (I), and a linear tissue impedance (Z_{Lti}). Hantos et al. (8) previously described Z_{Lti} as

$$Z_{Lti}(\omega_n) = \frac{(G - jH)}{\omega_n^{\alpha}}, \quad \text{with } \alpha = \frac{2}{\pi}\arctan\frac{H}{G} \qquad (1)$$

where ω is circular frequency and $\omega_n = \omega/\omega_0$. The normalization factor $\omega_0 = 1$ radian/s is used to obtain meaningful units for the parameters G and H. The parameters G and H are the coefficients of tissue damping and elastance, respectively, and the exponent α describes the frequency dependence of tissue resistance [$Rti = G/(\omega/\omega_0)^{\alpha}$] and tissue elastance [$Eti = H(\omega/\omega_0)^{1-\alpha}$]. In the model, the resistances are varied in each compartment according to a hyperbolic distribution function n(R), where n(R) is proportional to 1/R and R varies between R_a and R_b. By minimizing the root mean square difference between the model and the data, five parameters (G, H, R_a, R_b, and I) that characterize the macroscopic mechanics were determined. Additionally, hysteresivity (η) was calculated as the ratio of G to H, airway resistance (Raw) was taken as the mean value of the distribution function n(R) as a function of R_a and R_b, and heterogeneity was characterized by the standard deviation of n(R) (SDR). Hence

$$\text{Raw} = \int_{R_a}^{R_b} \text{Rn(R)dR} = \frac{R_b - R_a}{\ln R_b - \ln R_a} \qquad (2)$$

$$\text{SDR} = \sqrt{\int_{R_a}^{R_b} (R - \text{Raw})^2 n(R)\,dR} = \sqrt{\frac{(R_b^2 - R_a^2)}{2(\ln R_b - \ln R_a)} - \frac{(R_b - R_a)^2}{(\ln R_b - \ln R_a)^2}} \qquad (3)$$

Tissue preparation. Lung tissue strips ($n = 5$ control, $n = 3$ emphysematous) were prepared as in Kononov et al. (11). Briefly, thin strips ($0.4 \times 5 \times 5$ mm) of subpleural parenchyma were prepared by first infusing the lung with a 2% agarose solution at 55°C and allowing it to cool at room temperature. Thin strips were cut by using a vibratome, and the agarose was washed out. The tissue strips were then immunohistochemically labeled to view the alveolar walls. Anti-collagen type I or anti-elastin (Sigma Chemical) was diluted 1:2,000 or 1:5,000, respectively, in PBS, and the tissue strips were immersed in 800 μl of the primary antibodies at 37°C for 1 h. The strips were then washed three times in 1 ml of PBS at 20-min intervals and immersed in 800

μl of anti-mouse IgG FITC conjugate (Sigma) diluted 1:1,400 and incubated at 37°C for 1 h. The samples were again washed three times in 1 ml of PBS at 20-min intervals.

Microscopic imaging. The labeled tissue strips were fixed on one end to a metal plate with cyanoacrylate glue and connected to a servo-controlled lever arm (series 308B; Cambridge Technologies) with a steel wire. The other end was attached to a glass coverslip, which remained in a fixed position. The setup was attached to an acrylic base, and the entire apparatus was fit atop an inverted fluorescent microscope (Zeiss Axiovert 100TV). The samples were positioned over an opening just above the objective, and they were placed in saline with a coverslip creating the bottom of the tissue bath. The lever arm was used to quasi-statically apply a given strain to the tissue, and the same region was followed with the microscope during both the loading and unloading portions of the cycle. The reference state of 0% strain was defined as the strain just before that at which force was developed in the tissue strip. With the use of a charge-coupled device camera, images were captured of the alveolar wall network from 0 to 30% strain in increments of 10%. The collagen- and elastin-labeled strips were grouped together because at the resolution of these images the labeled structures correspond to the entire alveolar wall rather than individual collagen or elastin fibers (11).

Image processing. The diameters of the alveolar spaces were measured in the normal and emphysematous tissue strips at 0% strain to verify that the elastase treatment caused structural changes characteristic of emphysema. Then, as shown in Fig. 1, individual alveolar wall segments were followed throughout the elongation, and their length and orientation were manually measured by using SigmaScan Software (Jandel Scientific, San Rafael, CA). Figure 1*A* was taken at 0% strain, whereas Fig. 1*B* was taken of the same region at 30% strain. The local microstrain of individual alveolar walls was defined as the change in length of the alveolar wall normalized by the original length. Similarly, the orientations of the alveolar walls were characterized by measuring the change in angle of each alveolar wall segment with respect to the direction of macroscopic strain. The changes in length and angle of individual alveolar walls were analyzed as a function of macroscopic strain. To examine a general trend in the data without the influence of the most extreme cases, we averaged the measurements taken from line elements with an original angle of $<45°$ with respect to the direction of strain. These elements, which comprised roughly half of the total, provided us with the most reliable microstrain measurements.

Network simulation. To interpret the collective behavior of the alveolar walls in the parenchyma, a computer simulation of a two-dimensional network was developed based on the model introduced by Mishima et al. (20). The network consisted of a 20×20 hexagonal lattice connected by line elements. The line elements were modeled as imperfect prestressed springs capable of stress relaxation or adaptation. During loading, the network was stretched to 30% strain in increments of 10%, and the equilibrium configuration of the network was found at each increment by minimizing the total elastic energy of the network using simulated annealing (20). To simulate the relaxation, the initial length of each element was increased and the equilibrium configuration of the network was found again. This process therefore decreased the force on the elements. During the deformations, the border nodes were fixed while the internal nodes were free to move. Next the strain was increased again, and the system was relaxed as above. After relaxation, at each level of strain, the coordinates of the nodes were recorded, and therefore the length of each line element could be measured at each strain. During unloading, the macroscopic strain was decreased in increments of 10%, and the elements underwent stress adaptation by decreasing the initial length of the elements. Again the coordinates of each line element were recorded at each macroscopic strain.

The network simulation was first run for a homogeneous case, in which each line element underwent identical relaxation and adaptation of 20% of the initial length. Heterogeneity was then introduced by allowing the elements to undergo relaxation or adaptation with a standard deviation of 20% of the mean at each incremental strain. Using the coordinates, we calculated and plotted the length microstrain of each line element vs. the macroscopic strain to obtain plots analogous to the microstrain plots from individual alveolar walls. These simulations allowed us to examine the microstrains of each element as functions of macrostrain during cyclic loading for both a homogeneous and a heterogeneous case.

Statistical analysis. Data were expressed as means ± SE. For the impedance measurements, the differences in model parameters (i.e., G, H, η, Raw, SDR) between normal and emphysematous animals were tested by using two-way repeated-measures ANOVA. Data on hysteresivity from the separate populations were analyzed by using one-way re-

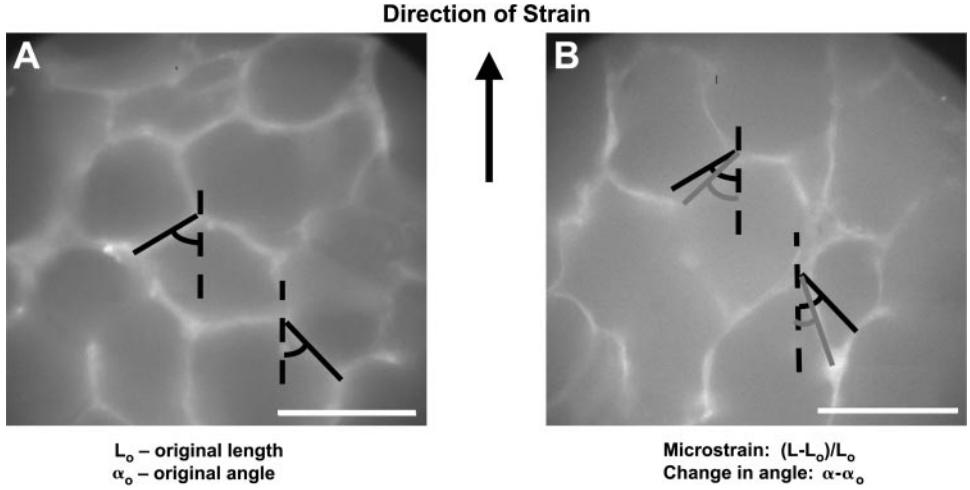

Fig. 1. An example of the measurements of microstrain and change in angle of individual alveolar wall segments. At 0% strain (*A*), the alveolar wall segments are traced and their lengths (L_o) and angles with respect to the direction of strain (α_o) are measured. At 30% strain (*B*), the new lengths (L) and angles (α) are measured. Microstrain is defined for each segment as the change in length divided by the length at 0% strain, and change in angle is the current angle minus the angle at 0% strain. Bar = 100 μm. Note that α here is different from α in *Eq. 1*.

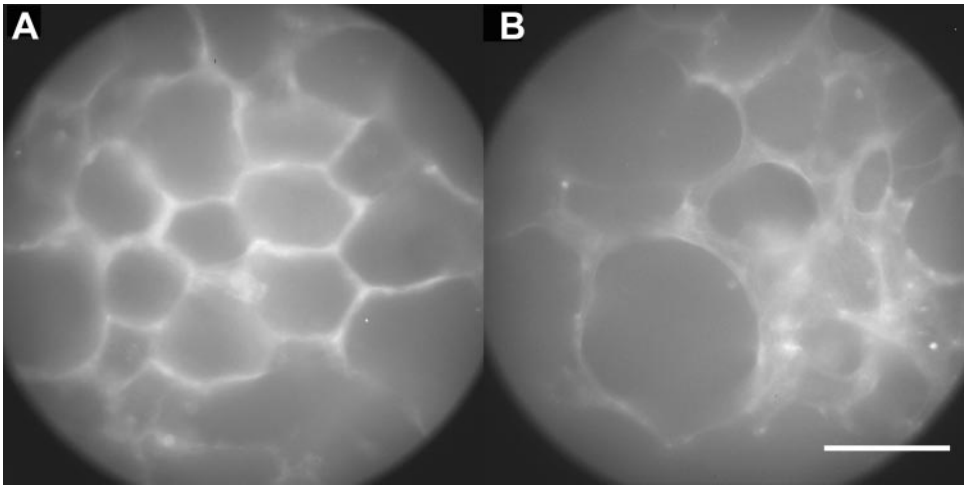

Fig. 2. Examples of fluorescently labeled lung tissue from normal (*A*) and elastase-treated (*B*) lungs. Bar = 100 μm.

peated-measures ANOVA and linear regression. The microscopic parameters measured were the microstrain and change in angle of individual alveolar walls. *t*-Tests were used to compare the slopes of the changes in angle vs. macroscopic strain. The measured changes in angle of the normal and emphysematous groups were compared by using Kruskal-Wallis one-way ANOVA on ranks. Differences between groups were considered statistically significant at $P < 0.05$.

RESULTS

Representative images from normal and emphysematous tissue strips at 0% strain are shown in Fig. 2, *A* and *B*, respectively. It can be seen that elastase treatment caused structural changes within the tissue (Fig. 2*B*) compared with the normal tissue (Fig. 2*A*). The treatment resulted in a relatively small (~19%) increase in mean linear intercept, or the distance between alveolar walls (90 ± 21 vs. 76 ± 22 μm), which, however, was statistically highly significant ($P < 0.005$), suggesting mild or early emphysema.

Examples of the impedance data collected from isolated lungs of a normal and an elastase-treated animal are shown in Fig. 3. The real and imaginary parts of the impedance were fit with the inhomogeneous linear model for both cases. The real part of the impedance is the resistance (Fig. 3*A*), whereas the elastance is calculated as the product of the imaginary part and $-2\pi f$, where f is frequency (Fig. 3*B*). The resistance of the emphysematous lung is higher and the elastance is substantially lower than that of the control lung, indicating loss of elastic recoil in the lungs of those animals treated with elastase. The model fits the data well, and the five model parameters (G, H, R_a, R_b, and I) were obtained from these fits.

Figure 4 shows the macroscopic mechanical properties of the normal and emphysematous isolated lungs. The parameters H, G, and η are shown at different levels of Ptp. The elastance of the normal lungs increased rapidly with Ptp, whereas in the treated lungs elastance increases at a much slower rate (Fig. 4*A*). The parameter H was found to significantly depend on both condition (normal or emphysematous) and Ptp, and there was a significant interaction between the two factors. The average slope of the linear regression of elastance vs. Ptp for the normal lungs (0.55) was significantly higher ($P < 0.01$) than for the emphysematous lungs (0.21). The damping parameter G for the

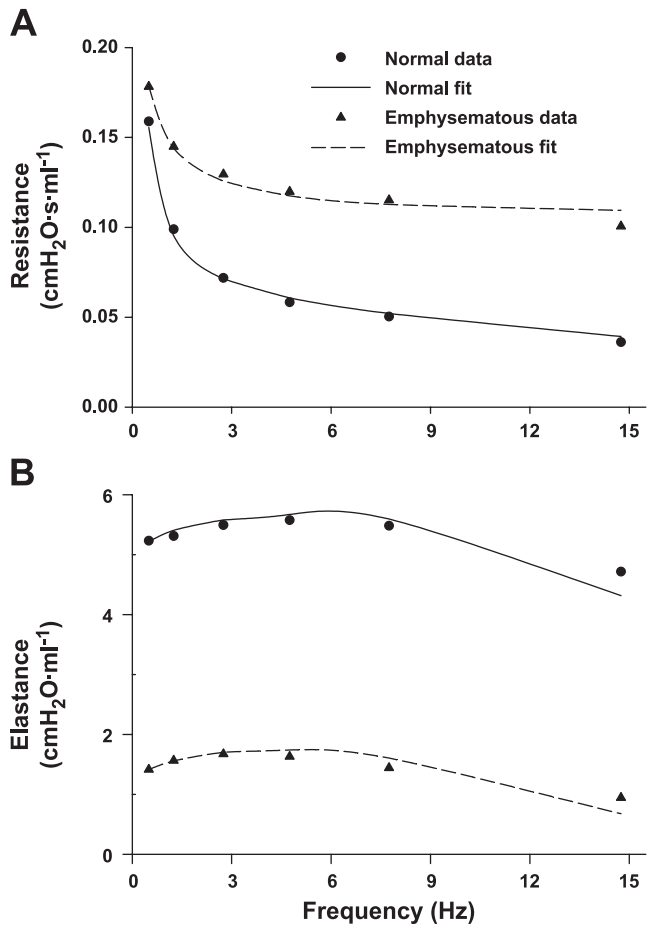

Fig. 3. Examples of resistance (*A*) and elastance (*B*) of normal and emphysematous lungs calculated from the impedance data at a transpulmonary pressure (Ptp) of 8 cmH_2O. Data (symbols) and fits (lines) of the inhomogeneous linear model are shown for the isolated lungs.

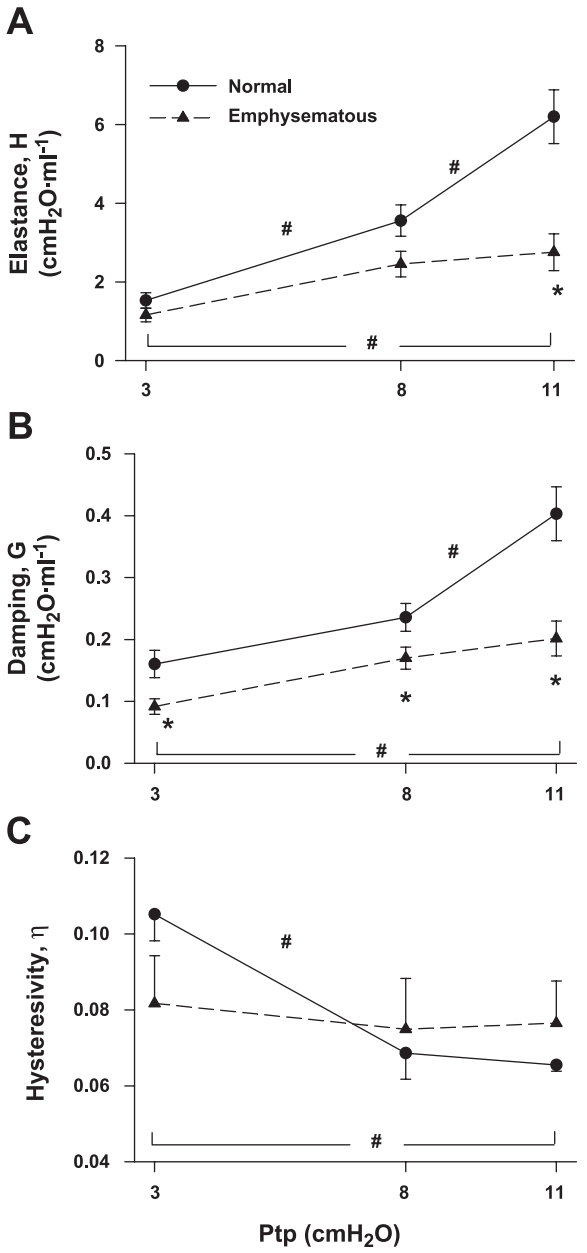

Fig. 4. Macroscopic mechanical properties of the normal and emphysematous isolated lungs. Elastance (*A*), damping (*B*), and hysteresivity (*C*) are shown as functions of Ptp. Data are shown as means ± SE. #Statistically significant between different levels of Ptp; *statistically significant between treatment groups (condition) ($P < 0.05$).

normal and emphysematous lungs showed a similar behavior (Fig. 4*B*). G significantly depended on both condition and Ptp, and the interaction between condition and Ptp was also statistically significant. The average slope of the linear regression of G vs. Ptp for the normal lungs (0.029) was more than twice that of the emphysematous lungs (0.014), and this difference was statistically significant ($P < 0.02$). With the use of two-way ANOVA on the entire population, hysteresivity was found to significantly depend on Ptp ($P < 0.02$), but no difference was detected with condition (Fig. 4*C*). However, by using one-way ANOVA on the separate populations of normal and treated lungs, hysteresivity was found to depend on Ptp for the normal lungs ($P < 0.002$) but not for the emphysematous lungs (Fig. 4*C*). In agreement with this test, linear regression showed that the slope of η vs. Ptp for the normal lungs was statistically significantly different from zero ($P < 0.0005$), whereas that for the emphysematous lungs was not different from zero. Therefore, hysteresivity did not decrease with Ptp in emphysematous lungs, whereas there was a systematic decrease in hysteresivity with Ptp in normal lungs.

Figure 5 shows a comparison of the population averages of Raw and the corresponding SDR for the normal and emphysematous lungs. At every Ptp, mean Raw was higher in the emphysematous case (Fig. 5*A*). Also, mean SDR was higher for the emphysematous lungs at every Ptp, indicating a larger degree of heterogeneity (Fig. 5*B*). Although these changes did not reach statistical significance, a trend of increased Raw and SDR for emphysematous lungs is evident.

To assess the microscopic origins of elastic and hysteretic behavior at the level of the alveolar wall, selected regions of the immunofluorescently labeled tissue strips were imaged while the macroscopic strain was increased from 0 to 30% and then decreased back to 0% strain. Figure 6 shows images from a selected region of normal lung tissue immunofluorescently labeled for elastin and stretched uniaxially in the vertical direction. The *top* row of images corresponds to the loading of the tissue, and the *bottom* row shows the

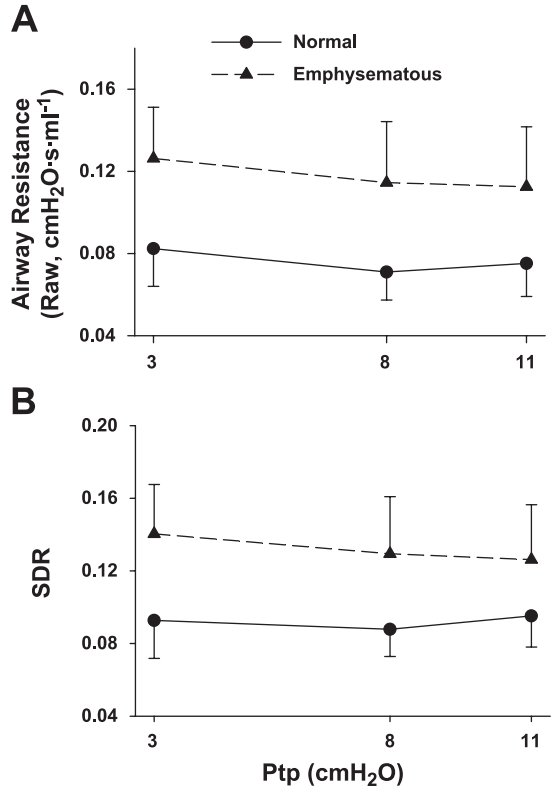

Fig. 5. Airway resistance (*A*) and standard deviation of resistance (SDR; *B*) are shown as functions of Ptp for the normal and emphysematous isolated lungs. Data are shown as means ± SE.

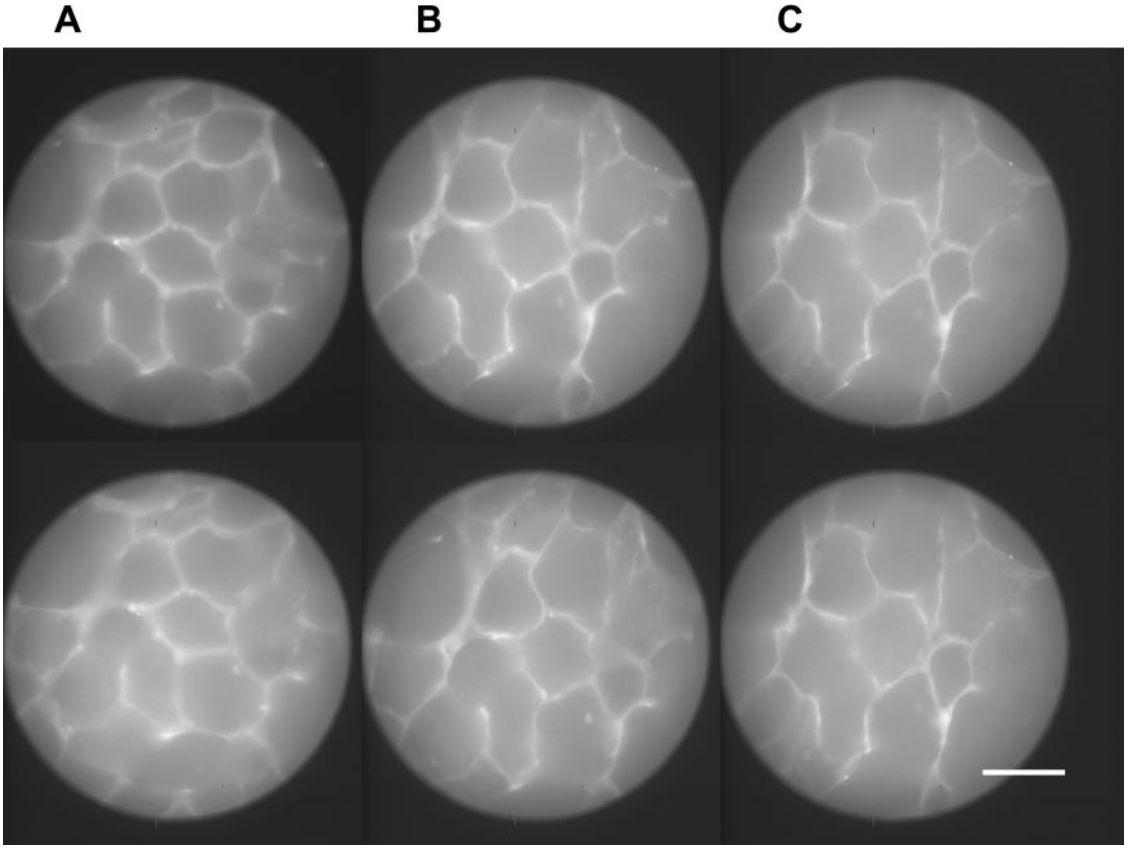

Fig. 6. An example of a series of microscopic images of normal lung tissue strips. The fluorescent (white) areas represent the alveolar walls. The *top* series shows the same region of tissue during loading at 0 (*A*), 20 (*B*), and 30% (*C*) strain, and the *bottom* series shows the same region at the same strains during unloading. The macroscopic strain is in the vertical direction. Bar = 100 μm.

same region during unloading. The network of alveolar walls appeared as an isotropic hexagonal mesh at 0% strain. As the tissue was stretched, the hexagons became distorted and the lengths and angles with respect to the direction of strain noticeably changed. From these images, the microstrains and changes in angle of the individual alveolar walls were calculated as in Fig. 1.

The microstrain and change in angle were plotted against macroscopic strain for each individual alveolar wall segment identified. Extreme heterogeneity was seen among these measurements; some of the microstrain loops followed a clockwise pattern, others a counterclockwise pattern, and some loops even followed a "figure-8" pattern. Examples of these patterns for individual alveolar wall segments are shown in Fig. 7. Each type of pattern was seen with similar frequency for both normal and emphysematous alveolar walls. The physiological implications of the heterogeneous behavior of the alveolar walls are further considered in DISCUSSION.

We next considered only the subset of alveolar wall segments that had an original angle of $<45°$. Figure 8 shows the average behavior of these normal and emphysematous alveolar walls during quasi-static stress-strain loops. Although the microstrain of individual segments may not have returned to the original microstrain when the macroscopic strain returned to zero, the average microstrain did return to zero. In contrast to the large hysteresis in the microstrain-macrostrain of individual walls seen in Fig. 7, the average hysteresis in length was negligible for both the normal and treated lungs. However, for the same macroscopic strain the alveolar walls for the treated lungs appeared to stretch more (Fig. 8*A*), although this increase did not reach statistical significance.

The angular hysteresis was notably larger in the treated lungs, but due to the extreme heterogeneity, this difference was not statistically significant. Additionally, the magnitudes of the angular changes of the treated lungs were smaller than those of the normal lungs (Fig. 8*B*), and the difference nearly reached a significant level ($P = 0.052$). The change in angle is a measure of how the alveolar walls fold with macroscopic strain. Figure 8*B* shows that, on average, alveolar walls fold to a lesser extent in the treated tissue. The linear regression slopes of the loading curves for individual wall segments were also compared, and the magnitudes of the slopes of the change in angle vs. macroscopic strain for the normal tissue were slightly larger than those for the emphysematous tissue. The dotted lines in Fig. 8*B* show the average theoretical change in angle for the normal and emphysematous alveolar walls if each wall followed continuum behav-

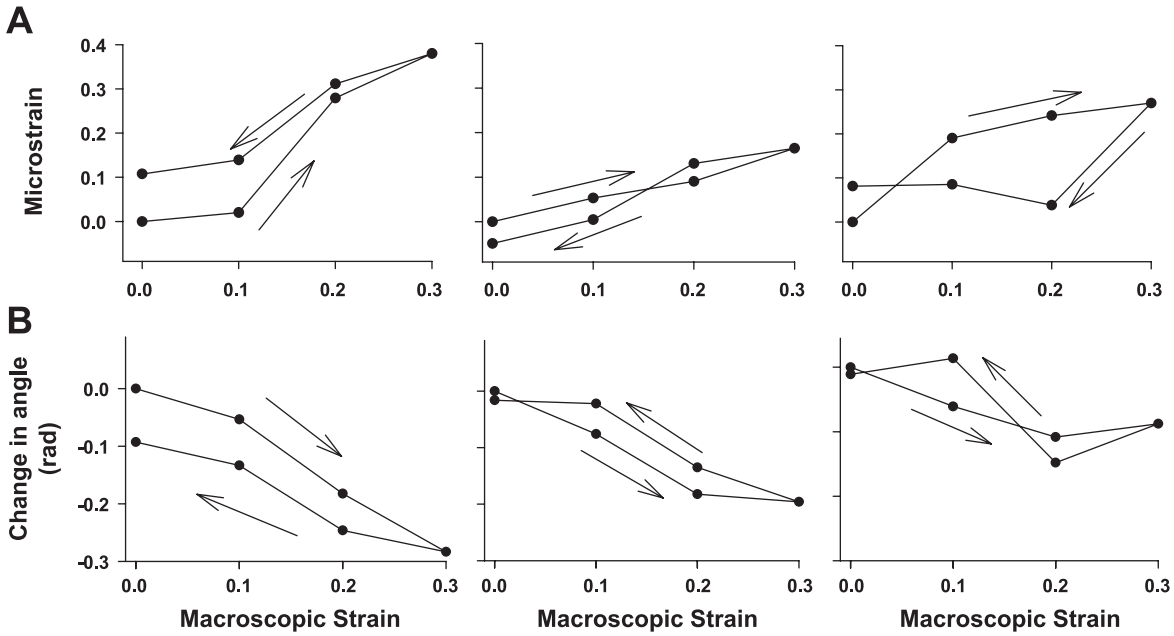

Fig. 7. Examples of microscopic measurements to determine the behavior of individual alveolar walls during macroscopic deformation. The microstrain (*A*) and change in angle (*B*) are plotted vs. macroscopic strain for 3 different segments. The measurements show various patterns of stretching and reorientation, indicating extreme heterogeneity. Note the "figure-8" patterns seen in many loops. The arrows indicate the direction of the loops.

ior based on its actual original angle and assuming that the Poisson's ratio (ν) = 0.5 (see APPENDIX).

The purpose of the computer simulation using the hexagonal network model was to better understand the heterogeneous folding pattern of the alveolar wall network. When each line element was assigned an equal relaxation and adaptation (homogeneous case), no hysteresis was observed in the microstrain vs. macrostrain curves, i.e., the loading and unloading portions of each element followed the same path (not shown). However, when we introduced heterogeneous relaxation into the network model by allowing a standard deviation of 20% in the mean relaxation and adaptation of the force on each element, various types of loop patterns were observed (Fig. 9). With heterogeneities, the same types of loop patterns were seen in the network as in the alveolar wall network, including the figure-8 pattern.

DISCUSSION

The main findings of our study are that in vivo elastase treatment caused changes in both the elastic and hysteretic properties of the whole lung and in the behavior of alveolar walls. Specifically, despite the small increase in mean linear intercept (~19%), the elastase treatment leads to a significant decrease in lung elastance as well as changes in the Ptp dependence of elastance. Additionally, the dependence of hysteresivity on Ptp was eliminated in the treated lungs. On the microscopic level, the alveolar walls of the treated tissue tended to be more extensible, and alveolar walls folded less in the treated tissue. However, this folding tended to have more hysteresis in the treated tissue than in the normal tissue. Before discussing the physiological implications of these

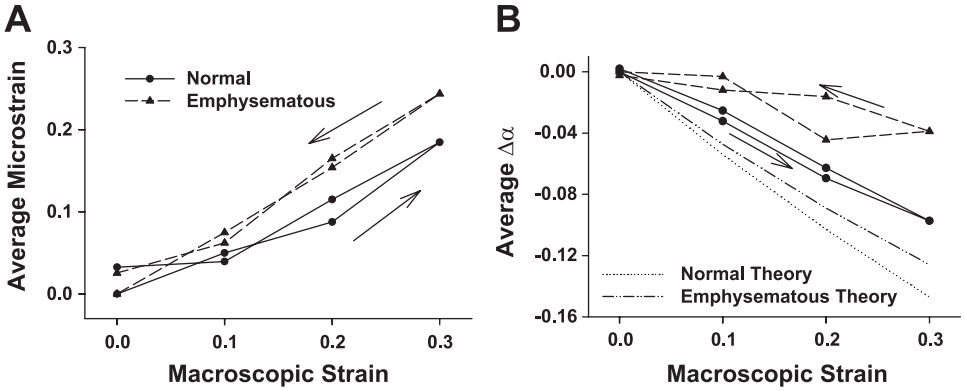

Fig. 8. Average behavior of the alveolar walls in the normal and emphysematous tissue strips. The average microstrain (*A*) and change in angle ($\Delta\alpha$; *B*) are shown as functions of macroscopic strain. Data are the averages of those alveolar wall segments whose original angle (at 0% macroscopic strain) was <45° with respect to the direction of macroscopic strain. The dotted lines show the theoretical averages for normal and emphysematous alveolar walls if each wall followed a continuum behavior.

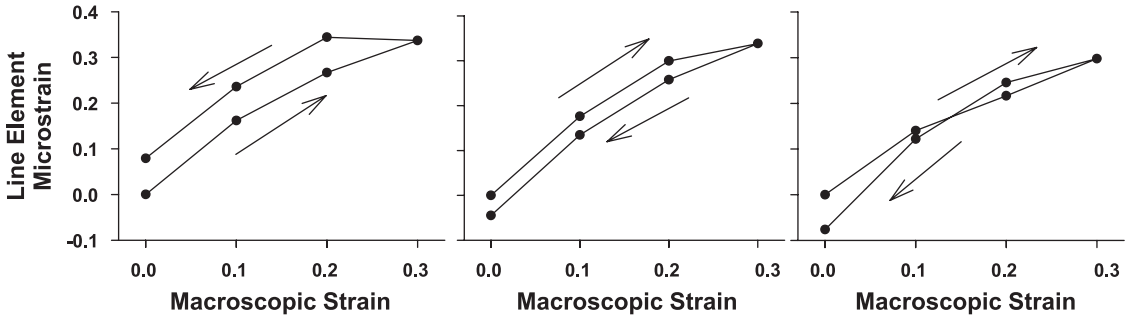

Fig. 9. Line element microstrain vs. macroscopic strain for select individual line elements of the hexagonal network model with 20% heterogeneity in relaxation and adaptation. The arrows indicate the direction of the loops.

changes, several methodological factors need to be considered.

Methodological considerations. The microscopic images of the alveolar walls portray a three-dimensional network in a single plane. Therefore, it is difficult to determine how the components move relative to the focal plane during stretching. To eliminate the corresponding uncertainty in the measurements, we considered only those alveolar wall segments whose intensity remained relatively constant throughout the stretching cycle. Also, there was extreme heterogeneity in the measurements. Segments in the direction of strain demonstrated considerable deformations, whereas those aligned perpendicular to the strain field remained relatively unchanged. To determine general trends, we did not evaluate segments that were generally perpendicular to the direction of strain because the displacement signals of these elements were not great enough to override the noise in the manual measurement of line element length and angle. As a result, the number of remaining segments included in the analysis was not always enough to overcome the inherent heterogeneity at the microscopic level and to obtain statistically significant results. However, for both the length-microstrain and change-in-angle measurements, the standard deviation from the mean was larger in the emphysematous tissue than the normal tissue at every level of macroscopic strain.

Another drawback of the tissue preparation method used to collect the microscopic data is the possible effects of agarose inflation on tissue strip mechanics. As described, the lungs were infused with agarose at 55°C to enable even slicing of thin tissue strips. Although the strips were then heated to 55°C to remove the agarose, some agarose may have remained in the tissue and could have affected the nature of the alveolar wall folding during stretching. However, since the normal and emphysematous strips were treated identically, the effect of the agarose was the same for all strips and therefore should have a minimal effect on the comparisons made here.

A gap in information clearly exists between the mechanical properties measured from isolated lungs and the microscopic observations of thin tissue strips. The active surface forces present at the air-liquid interface in isolated lungs are excluded in tissue strips, and the mechanics are therefore likely to be different (22). Also, different-sized alveoli in situ will create different forces on the two sides of the wall, which would further increase these forces. Additionally, organ-level mechanical measurements involve three-dimensional uniform expansion of the lung, whereas in the tissue strips uniaxial deformations are applied. Despite these limitations, Kononov et al. (11) previously measured the stress-strain curves of normal and elastase-treated thin tissue strips, and the behavior was qualitatively similar to that found in the pressure-volume curves of the respiratory system.

Macroscopic mechanics. The Ptp dependence of elastance and hysteresivity in the normal rats is in agreement with several previous studies of lung tissue mechanics. Sly et al. (28) studied dynamic lung mechanical parameters by applying small-amplitude forced oscillations in normal mice. Measurements were made at several different transrespiratory pressures, and a decrease in hysteresivity was shown with increasing lung volume. This decreasing hysteresivity was similar to that found by Sakai et al. (26) in normal rats. Sly et al. (28) also argued that the lung volume-dependent nature of hysteresivity could be attributed to the progressive contribution of collagen at higher lung volumes. Since the hysteresivity of collagen is less than that of elastin (18, 36), it follows that at higher lung volumes, as collagen plays a larger role, the hysteresivity of the lung will decrease. A statistically significant decrease in hysteresivity with Ptp was seen in the normal animals from our study as well (Fig. 4*C*).

In another study, Pillow et al. (25) showed that the development of structural emphysema influences parenchymal hysteresivity. The mechanical properties of lungs from normal mice were compared with those from transgenic mice overexpressing transforming growth factor-α, which creates structural lung disease characterized by abnormally large alveolar spaces. Their study showed a trend of decreasing elastance without a significant increase in hysteresivity in the mice with alterations in lung structure compared with normal mice. These findings are consistent with our findings: in our elastase-treated group hysteresivity did not decrease with increasing Ptp, and hysteresivity was larger in the treated animals at high levels of Ptp. This change is likely due to real changes in the hyster-

etic properties of the alveolar connective tissue of the treated animals.

We investigated the effects of heterogeneities on lung mechanics by fitting the impedance data using a model that includes parallel heterogeneities (32). Although not statistically significant, Raw and SDR indeed tended to increase in the emphysematous lungs, indicating that the treatment caused heterogeneous changes in the macroscopic lung properties (Fig. 5). In principle, an increase in hysteresivity observed at the organ level may reflect heterogeneities (26). However, since we included heterogeneities in our model of lung impedance, the altered Ptp dependence of hysteresivity in the treated group cannot be solely due to heterogeneities. In the normal lungs, the decrease in hysteresivity is due to the increased contribution of collagen fibers at higher levels of Ptp (28). In the treated lungs, the fact that hysteresivity does not decrease with Ptp indicates that structural changes induced by elastase treatment may create remodeled fibers, especially collagen, with different hysteretic properties. It has been reported that, following elastase treatment, collagen undergoes remodeling (12) and can even rupture (11). Because the increasing contribution of collagen is responsible for the steep rise of elastance with Ptp in the normal lungs, the remodeled collagen must be responsible for the plateau of elastance with increasing Ptp in the emphysematous lungs. The organ-level changes in mechanics could thus be due to remodeling of elastin and collagen or mechanical failure of collagen, or perhaps both, which are discussed in *Microscopic mechanics*.

Microscopic mechanics. The most accepted characterization of the development of emphysema is the measurement of mean linear intercept on histological sections of lung tissue. The significant increase seen in the mean linear intercept of elastase-treated lungs is due to destruction of alveolar walls, often causing two or more alveoli to coalesce into one (17, 23). The mean alveolar diameters increased in our treated group, confirming the development of structural emphysema. Recently, Kononov et al. (11) developed a technique to measure how alveolar diameters change during uniaxial stretching and concluded that mechanical forces contribute to the destruction of lung tissue. In this study, we further developed this technique, which is unique in that it allowed us to visualize and quantify the microscopic manifestations of in vivo elastase treatment during quasi-static cyclic stretching. Thus we could investigate how changes in the connective tissue matrix contribute to the dynamic organ-level mechanical properties.

It is well established that emphysema causes a decrease in lung elastance. Since elastance also decreases in tissue strips, which exclude the air-liquid interface, the alveolar walls themselves should be more easily extensible in the emphysematous tissue. Indeed, for the same macroscopic strain, the alveolar walls from the elastase-treated tissue show a larger microstrain in length (Fig. 8*A*). However, the microstrain was not statistically larger in the treated tissue than in the normal tissue. The reason for this is likely related to the large heterogeneity or the network behavior (see *Network behavior*, below) observed at the level of the alveolar walls. There are two ways a hexagonal structure can accommodate strain: it can stretch via elongation of the line elements or it can fold by changing the angles between adjacent line elements. Although the alveolus is hexagon-like, when it was stretched uniaxially we observed changes both in angle and in wall segment length (Fig. 1). Because the normal tissue is stiffer and the alveolar walls are less extensible, the walls of the normal tissue are more likely to accommodate stretch by changing orientation. Indeed, the normal tissue showed a larger absolute change in angle than the emphysematous tissue. Thus, although heterogeneity was sufficiently large to eliminate statistical differences in length-related microstrains and angular changes between normal and treated tissue, the trends suggest that alveolar walls are more extensible in the elastase-treated tissue.

Neither the normal nor the emphysematous alveolar walls exhibited hysteresis in average length microstrain (Fig. 8*A*). However, on closer examination of the individual loop patterns in Fig. 7, it is apparent that the reason for this lack of hysteresis is the presence of extreme heterogeneity in the loop behavior. In contrast to measurements of length microstrain, on average the emphysematous tissue showed a much larger hysteresis area in the angle change measurements than the normal tissue (Fig. 8*B*), but the larger hysteresis area in the treated tissue was not statistically significant. The lack of statistical significance is again very likely due to the variety of behaviors seen in the loops for individual alveolar walls, suggesting that, besides the properties of the individual alveolar walls, the network behavior plays an important role in the behavior of each segment. The increased microscopic angular hysteresis likely contributes to the increased hysteresivity seen in the treated isolated lungs at high levels of Ptp.

In a network, the heterogeneous viscoelastic properties of neighboring segments can significantly contribute to a segment's microscopically observed mechanical behavior. The deformation and folding of an isolated segment can behave differently from a segment that is part of a network. This strong network effect appears to suggest that individual alveolar walls may not follow the continuum macroscopic strain field. To quantify this network effect, we calculated the expected changes in angles that would occur if the folding of individual alveolar walls followed the macroscopic strain field (see APPENDIX)

$$\Delta\alpha = -\arctan\left[\frac{\varepsilon(1+\nu)\sin\alpha_0\cos\alpha_0}{1+\varepsilon(\cos^2\alpha_0-\nu\sin^2\alpha_0)}\right] \qquad (4)$$

where ε is the macroscopic strain, α_0 is the original angle of the segment with respect to the macroscopic strain, and ν is Poisson's ratio (see Fig. 1).

Figure 8*B* shows the averages of the measured changes in angle vs. the macroscopic strain, along with lines representing the predicted changes in angle (us-

ing $\nu = 0.5$ in *Eq. 4*) for the normal and emphysematous alveolar walls. The predicted change in angle including all macroscopic strains and both conditions was -0.092 ± 0.055 radians, whereas the corresponding measured change in angle was -0.044 ± 0.118 radians, and the difference was highly significant (paired *t*-test; $P < 0.001$). Also, the variability of the measured changes in angle was 100% larger than that of the predicted changes in angle (*F*-test; $P < 0.001$). In a previous study, Butler et al. (2) found that the average microscopic strain closely matched the macroscopic strain field during uniaxial distortion. They superimposed the uniaxial shear deformation on a uniformly prestressed state of the air-filled lung, which homogenized the system, whereas our tissue strips submerged in fluid started from an unstressed state. Additionally, Butler et al. (2) considered length scales of 1–2 cm sampled by an optical probe, and their data may correspond to the average behavior of several hundred alveoli. In this study, we have examined the mechanics of individual alveolar walls at length scales of about two orders of magnitude smaller than those of Butler et al. (2). Our results suggest that continuum analysis cannot be used to evaluate the configurations of the individual alveolar walls and that network models must be used to describe the behavior instead.

Network behavior. To interpret the experimentally observed loop patterns of the alveolar walls (Fig. 7), we used a computer simulation of a two-dimensional hexagonal network model to represent the alveolar wall network (20). This model was not intended to faithfully model the parenchyma, but it is useful to gain a qualitative understanding of the mechanical behavior of an interconnected heterogeneous structure. Indeed, with heterogeneous relaxation invoked in the model, the behavior of the network elements mimicked the behavior of the individual alveolar walls in the tissue strips. Some line elements even showed the figure-8 pattern (Fig. 9*C*). The heterogeneous relaxation gives each element different properties to simulate the fact that each alveolar wall segment may have a slightly different composition, and therefore each will respond differently to the imposed strain. Also, the observed behavior of each alveolar wall is dependent on the behavior of neighboring walls. Hence, we conclude that network behavior plays an important role in the observed mechanical behavior of individual wall segments, which therefore cannot be characterized in isolation from their neighbors.

Additional network effects can result from mechanical failure of the alveolar walls. Along with enzymatic digestion of elastin fibers, the development of emphysema initiates various biochemical cascades, resulting in elastin and collagen remodeling (12, 17, 33). Fatigue and ultimately failure of weakened individual fibers and entire alveolar walls is likely to occur during cyclic stretching similar to breathing (11). Destruction of alveolar walls changes the stress distribution and dissipation of the tissue. Indeed, if rupture occurs somewhere in the network during cyclic stretching, increased hysteresis may be observed in the microscopic behavior of individual segments. Additionally, failure of alveolar walls at high strains may also contribute to the plateau of elastance at high levels of Ptp. Thus during emphysema, changes in the structural composition of the tissue as well as network failure should be reflected in changes in elasticity and hysteresivity.

Conclusions. By studying lung tissue mechanics on both macroscopic and microscopic levels, we have found that, whereas the normal lungs showed a decrease in hysteresivity with Ptp, the emphysematous lungs showed a constant hysteresivity at all Ptp levels. Additionally, lung elastance was lower and showed a significantly reduced dependence on Ptp in the treated animals. These functional alterations occurred despite the relatively small increase in mean linear intercept. Thus we suggest that the Ptp dependence of elastance and hysteresivity can signal the early remodeling of elastin and collagen fibers in the alveolar walls during the development of emphysema. By using a network model, we have also qualitatively described the large heterogeneity and distortions of the alveolar wall network during uniaxial deformation. We conclude that remodeling and possibly failure at the level of individual fibers in emphysema are important contributors to the altered mechanical properties of the entire lung. Future studies should focus on the mechanics of individual fibers within one alveolar wall and develop quantitative network models to bridge the scales from fiber and alveolar wall mechanics to lung behavior.

APPENDIX

The theoretical deformation of individual alveolar wall segments can be predicted by using mean field calculations

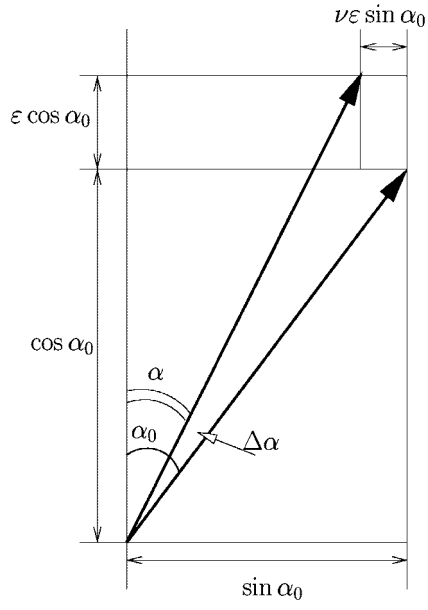

Fig. 10. Vectors representing the initial and final orientations of an alveolar wall segment with a Poisson's ratio (ν) and macroscopic strain (ε) in the vertical direction. The average $\Delta\alpha$ can be predicted if it is assumed that each segment follows the continuum. α_0, Original angle of the segment. Note that α, angle of segment after deformation, is different from α in *Eq. 1*.

as follows. Let us consider an elastic body undergoing vertical stretching. A line element in the body with unit length and angle of α_0 deforms by $\Delta\alpha$ under continuum strain (Fig. 10). The strain in the vertical direction is ε. Thus the vertical elongation is $\varepsilon \cos \alpha_0$. The horizontal strain is given by $-\nu\varepsilon$, where ν is Poisson's ratio and the corresponding shrinkage is $\nu\varepsilon \sin \alpha_0$. The tangent of the angle α following deformation is

$$\tan \alpha = \tan (\alpha_0 + \Delta\alpha) = \frac{\sin \alpha_0 - \nu\varepsilon \sin \alpha_0}{\cos \alpha_0 + \varepsilon \cos \alpha_0} \qquad (A1)$$

Expanding first the $\tan (\alpha_0 + \Delta\alpha)$ term and then using *Eq. A1* again, we obtain

$$\Delta\alpha = -\arctan \left[\frac{\varepsilon(1 + \nu) \sin \alpha_0 \cos \alpha_0}{1 + \varepsilon(\cos^2 \alpha_0 - \nu \sin^2 \alpha_0)} \right] \qquad (A2)$$

The above equation gives the expected change in angle for a given segment with initial angle α_0 if the segment follows the macroscopic strain field. Thus the average $\Delta\alpha$ from the measured data can be compared with the prediction of *Eq. A2* (Fig. 8*B*).

We thank Dr. J. P. Butler for helpful comments.

DISCLOSURES

This work was funded by National Heart, Lung, and Blood Institute Grant HL-59215.

REFERENCES

1. **Barnes PJ.** Chronic obstructive pulmonary disease. *N Engl J Med* 343: 269–280, 2000.
2. **Butler JP, Miki H, Squarcia S, Rogers RA, and Lehr JL.** Effect of macroscopic deformation on lung microstructure. *J Appl Physiol* 81: 1792–1799, 1996.
3. **Butler JP, Oldmixon EH, and Hoppin FG Jr.** Dihedral angles of septal "bend" structures in lung parenchyma. *J Appl Physiol* 81: 1800–1806, 1996.
4. **Di Stefano A, Capelli A, Lusuardi M, Balbo P, Vecchio C, Maestrelli P, Mapp CE, Fabbri LM, Donner CF, and Saetta M.** Severity of airflow limitation is associated with severity of airway inflammation in smokers. *Am J Respir Crit Care Med* 158: 1277–1285, 1998.
5. **Fredberg JJ, Bunk D, Ingenito E, and Shore SA.** Tissue resistance and the contractile state of lung parenchyma. *J Appl Physiol* 74: 1387–1397, 1993.
6. **Fredberg JJ and Stamenovic D.** On the imperfect elasticity of lung tissue. *J Appl Physiol* 67: 2408–2419, 1989.
7. **Fukuda Y, Masuda Y, Ishizaki M, Masugi Y, and Ferrans VJ.** Morphogenesis of abnormal elastic fibers in lungs of patients with panacinar and centriacinar emphysema. *Hum Pathol* 20: 652–659, 1989.
8. **Hantos Z, Daroczy B, Csendes T, Suki B, and Nagy S.** Modeling of low-frequency pulmonary impedance in dogs. *J Appl Physiol* 68: 849–860, 1990.
9. **Janoff A.** Elastases and emphysema. Current assessment of the protease-antiprotease hypothesis. *Am Rev Respir Dis* 132: 417–433, 1985.
10. **Jones PW.** Health status measurement in chronic obstructive pulmonary disease. *Thorax* 56: 880–887, 2001.
11. **Kononov S, Brewer K, Sakai H, Cavalcante FS, Sabayanagam CR, Ingenito EP, and Suki B.** Roles of mechanical forces and collagen failure in the development of elastase-induced emphysema. *Am J Respir Crit Care Med* 164: 1920–1926, 2001.
12. **Lucey EC, Goldstein RH, Stone PJ, and Snider GL.** Remodeling of alveolar walls after elastase treatment of hamsters. Results of elastin and collagen mRNA in situ hybridization. *Am J Respir Crit Care Med* 158: 555–564, 1998.
13. **Ludwig MS, Dreshaj I, Solway J, Munoz A, and Ingram RH Jr.** Partitioning of pulmonary resistance during constriction in the dog: effects of volume history. *J Appl Physiol* 62: 807–815, 1987.
14. **Lutchen KR, Yang K, Kaczka DW, and Suki B.** Optimal ventilation waveforms for estimating low-frequency respiratory impedance. *J Appl Physiol* 75: 478–488, 1993.
15. **Mead J, Takishima T, and Leith D.** Stress distribution in lungs: a model of pulmonary elasticity. *J Appl Physiol* 28: 596–608, 1970.
16. **Mead J, Whittenberger JL, and Radford J, EP.** Surface tension as a factor in pulmonary volume-pressure hysteresis. *J Appl Physiol* 10: 191–196, 1957.
17. **Mercer RR and Crapo JD.** Structural changes in elastic fibers after pancreatic elastase administration in hamsters. *J Appl Physiol* 72: 1473–1479, 1992.
18. **Mijailovich SM, Stamenovic D, Brown R, Leith DE, and Fredberg JJ.** Dynamic moduli of rabbit lung tissue and pigeon ligamentum propatagiale undergoing uniaxial cyclic loading. *J Appl Physiol* 76: 773–782, 1994.
19. **Mijailovich SM, Stamenovic D, and Fredberg JJ.** Toward a kinetic theory of connective tissue micromechanics. *J Appl Physiol* 74: 665–681, 1993.
20. **Mishima M, Hirai T, Itoh H, Nakano Y, Sakai H, Muro S, Nishimura K, Oku Y, Chin K, Ohi M, Nakamura T, Bates JH, Alencar AM, and Suki B.** Complexity of terminal airspace geometry assessed by lung computed tomography in normal subjects and patients with chronic obstructive pulmonary disease. *Proc Natl Acad Sci USA* 96: 8829–8834, 1999.
21. **Navajas D, Maksym GN, and Bates JH.** Dynamic viscoelastic nonlinearity of lung parenchymal tissue. *J Appl Physiol* 79: 348–356, 1995.
22. **Navajas D, Moretto A, Rotger M, Nagase T, Dallaire MJ, and Ludwig MS.** Dynamic elastance and tissue resistance of isolated liquid-filled rat lungs. *J Appl Physiol* 79: 1595–1600, 1995.
23. **Ofulue AF, Ko M, and Abboud RT.** Time course of neutrophil and macrophage elastinolytic activities in cigarette smoke-induced emphysema. *Am J Physiol Lung Cell Mol Physiol* 275: L1134–L1144, 1998.
24. **Oldmixon EH, Butler JP, and Hoppin FG Jr.** Lengths and topology of alveolar septal borders. *J Appl Physiol* 67: 1930–1940, 1989.
25. **Pillow JJ, Korfhagen TR, Ikegami M, and Sly PD.** Overexpression of TGF-α increases lung tissue hysteresivity in transgenic mice. *J Appl Physiol* 91: 2730–2734, 2001.
26. **Sakai H, Ingenito EP, Mora R, Abbay S, Cavalcante FS, Lutchen KR, and Suki B.** Hysteresivity of the lung and tissue strip in the normal rat: effects of heterogeneities. *J Appl Physiol* 91: 737–747, 2001.
27. **Schürch S, Bachofen H, Goerke J, and Green F.** Surface properties of rat pulmonary surfactant studied with the captive bubble method: adsorption, hysteresis, stability. *Biochim Biophys Acta* 1103: 127–136, 1992.
28. **Sly PD, Collins RA, Thamrin C, Turner DJ, and Hantos Z.** Volume dependence of airway and tissue impedances in mice. *J Appl Physiol* 94: 1460–1466, 2003.
29. **Snider GL.** Emphysema: the first two centuries—and beyond. A historical overview, with suggestions for future research: Part 1. *Am Rev Respir Dis* 146: 1334–1344, 1992.
30. **Snider GL, Lucey EC, and Stone PJ.** Animal models of emphysema. *Am Rev Respir Dis* 133: 149–169, 1986.
31. **Suki B, Barabasi AL, and Lutchen KR.** Lung tissue viscoelasticity: a mathematical framework and its molecular basis. *J Appl Physiol* 76: 2749–2759, 1994.
32. **Suki B, Yuan H, Zhang Q, and Lutchen KR.** Partitioning of lung tissue response and inhomogeneous airway constriction at the airway opening. *J Appl Physiol* 82: 1349–1359, 1997.
33. **Vlahovic G, Russell ML, Mercer RR, and Crapo JD.** Cellular and connective tissue changes in alveolar septal walls in emphysema. *Am J Respir Crit Care Med* 160: 2086–2092, 1999.
34. **Wilson TA.** A continuum analysis of a two-dimensional mechanical model of the lung parenchyma. *J Appl Physiol* 33: 472–478, 1972.
35. **Yuan H, Ingenito EP, and Suki B.** Dynamic properties of lung parenchyma: mechanical contributions of fiber network and interstitial cells. *J Appl Physiol* 83: 1420–1431, 1997.
36. **Yuan H, Konknov S, Cavalcante FS, Lutchen KR, Ingenito EP, and Suki B.** Effects of collagenase and elastase on the mechanical properties of lung tissue strips. *J Appl Physiol* 89: 3–14, 2000.